JOURNAL OF CHEMICAL INFORMATION AND MODELING

Article

pubs.acs.org/jcim

Extended Template-Based Modeling and Evaluation Method Using Consensus of Binding Mode of GPCRs for Virtual Screening

Miwa Sato[†,‡,§] and Takatsugu Hirokawa*[,‡]

[†]Department of Supramolecular Biology, Graduate School of Nanobioscience, Yokohama City University, Yokohama 230-0045, Japan

[‡]Molecular Profiling Research Center of Drug Discovery (molprof), National Institute of Advanced Industrial Science and Technology (AIST), Tokyo 135-0064, Japan

[§]Mitsui Knowledge Industry Co., Ltd., Tokyo 105-6215, Japan

Supporting Information

ABSTRACT: G-protein-coupled receptors (GPCRs) are a pharmaceutically important protein family because they mediate numerous physiological functions. The crystal structures of several GPCR subtypes have been determined recently, encouraging efforts to apply structure-based virtual screening (SBVS) along with ligand-based virtual screening (LBVS) to improve the hit rate of active ligands from large chemical libraries. Three-dimensional models are also necessary for GPCR targets whose structures are unknown. Current challenges include the selection of structural templates from available structurally known GPCRs to use for accurate modeling and understanding the diversity of sites recognizing distinct ligands. We have developed and validated an extended template-based modeling and evaluation method for SBVS. Models were generated using a fragmental template procedure in addition to typical template-based modeling methods. The reliability of the models was evaluated using a virtual screening test with known active ligands and decoys and the consensus of the binding mode using the protein−ligand interaction fingerprint (PLIF) derived from the results of docking simulations. This novel workflow was applied to three targets with known structures (human dopamine receptor 3, human histamine H1 receptor, and human delta opioid receptor) and to a target with an unknown structure (human serotonin 2A receptor). In each case, model structures having high ligand selectivity with consensus binding mode were generated.

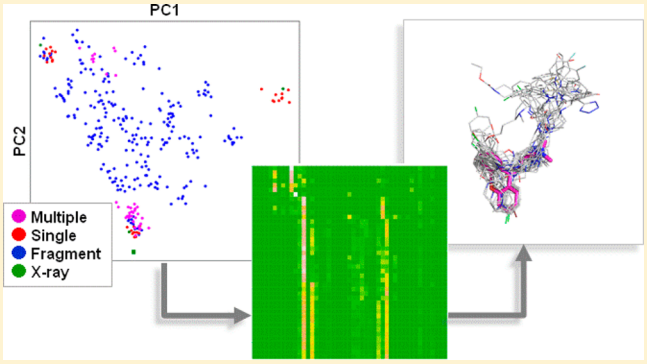

INTRODUCTION

G-protein-coupled receptors (GPCRs) form the largest membrane protein family in the human genome. Many GPCRs are drug targets because they play important roles in cellular signal transduction pathways.[1] GPCRs have a common topology composed of seven transmembrane helices (TMH), three intracellular loops (ICL), three extracellular loops (ECL), and domains at both ends. The number of experimental GPCR structures submitted to the Protein Data Bank (PDB) has been increasing since the release of the Rhodopsin X-ray structure in 2000 and particularly since 2010. Class A is the largest GPCR subfamily and contains most of the current drug targets.[2] High-resolution crystal structures have been reported to date for the following 21 class A GPCRs: (1) squid rhodopsin (sOPSD), (2) bovine rhodopsin (bOPSD), (3) turkey beta 1 adrenergic receptor (ADRB1), (4) human beta 2 adrenergic receptor (ADRB2), (5) human adenosine A2A receptor (AA2AR), (6) human dopamine receptor 3 (DRD3), (7) human histamine receptor H1 (HRH1), (8) human CXC chemokine receptor type 4 (CXCR4), (9) human muscarinic acetylcholine receptor M2 (ACM2), (10) rat muscarinic acetylcholine receptor M3 (ACM3), (11) human protease-activated receptor 1 (PAR1), (12) mouse and human delta-type opioid receptor (OPRD), (13) human kappa-type opioid receptor (OPRK), (14) human mu-type opioid receptor (OPRM), (15) human nociceptin/orphanin FQ receptor (OPRX), (16) rat neurotensin receptor type 1 (NTR1), (17) human CXC chemokine receptor type 1 (CXCR1, a structure determined by NMR), (18) human sphingosine 1-phosphate receptor 1 (S1PR1), (reviewed in ref 2) (19) human serotonin (5-hydroxytryptamine) receptor 1B (5HT1B),[3] (20) human serotonin (5-hydroxytryptamine) receptor 2B (5HT2B),[4] and (21) human chemokine receptor CCR5 (CCR5).[5] The first crystal structures of class B GPCRs, the human corticotropin-releasing factor 1 receptor (CRFR1) and the human glucagon receptor (GLR),[6] and the first crystal structure of a class F GPCR, human smoothened receptor (SMO),[7] were determined in 2013. Recently, structures of the transmembrane domain of a class C GPCR, metabotropic glutamate receptor 1 bound to an allosteric modulator,[8] and of the agonist-bound human P2Y12 receptor,[9] also have been determined.

Received: August 15, 2014

dx.doi.org/10.1021/ci500499j | J. Chem. Inf. Model. XXXX, XXX, XXX−XXX

These three-dimensional structures are useful for structure-based virtual screening (SBVS). However, they cannot be used to directly model GPCRs with unknown structures because (a) the total number of human class A GPCRs has been estimated to include about 800 receptors, (b) the sequence identities among these GPCRs are low,[10]and (c) each GPCR recognizes multiple ligands, some of which may be distinct and some of which may be recognized by other GPCRs. Therefore, almost all efforts to construct GPCR structures for virtual screening and ligand design have used prediction methods specialized for GPCRs, which take into account their characteristic common topology. Historically, two primary methods have been used to model GPCR structures. The first is a template-free modeling method to construct three-dimensional protein structures using amino acid sequence information and physicochemical properties. Examples of this approach include PREDICT,[11] MembStruk,[12] and BiHelix.[13] The second method is template-based modeling, which utilizes a known protein structure as a scaffold in the construction of the model structure. The latter method is well established, and numerous successes have been reported in SBVS studies.[14] In many cases, a suitable template was selected; however, the use of multiple templates often improved the quality of the resulting models.[15] The increasing number of experimental GPCR structures being submitted to the PDB is improving the quality of the modeled structures. This has also led to discussions of which crystal structures are most suitable for use as objective target templates. Generally, the sequence identity between target and template must be >40% to construct a reliable model, and this is especially necessary for SBVS. There is still an insufficient number of experimental GPCR structures to model all unknown targets of interest.[16] In addition, the use of the sequence similarity criteria alone does not guarantee selection of the best template. The GPCR-SSFE Database[17] served as a fragment-based model that was chosen based on results of comparative sequence and structural analyses. These analyses indicated the existence of sequence motifs that determined specific structural features.[18] However, in general, it is not clear whether the use of templates that are single, multiple, or fragment-based is most suitable to build specific models.

In the present study, in order to generate many credible candidates, an extended template-based GPCR modeling method that utilized seed fragments was used in addition to single and multiple templates. An assessment method was also devised to select the most suitable model structure for virtual screening from the many candidates thus generated. In general, three-dimensional structures that can distinguish active ligands from decoys are extracted via docking simulations and the receiver operating characteristic (ROC), which is calculated based on the docking score.[19] However, these docking algorithms do not distinguish between different possible binding modes for specific ligands. We therefore developed an evaluation indicator that takes into account consensus binding modes of ligands known to bind to GPCRs. The basis for these consensus binding modes is the earlier suggestion of an initial binding mode, as postulated by Graaf and Rognan[20] and by Wacker et al.[21] According to this theory, GPCR binding to ligands causes sequential conformational changes from the initial recognition of a ligand to binding of the GPCR to a G protein.[22] The initial recognition of a ligand is thus the first step in a cascade of conformational changes. An initial consensus binding mode to a pharmacophore has been confirmed by X-ray structure analyses of ADRB2 bound to pharmacologically distinct ligands such as an agonist, antagonists, and inverse agonists. All of these pharmacophores bound to highly similar overlapping sites in the same binding pocket.[2,23] We have developed an evaluation indicator, named Tc50, which calculates a protein ligand interaction fingerprint (PLIF) and its Tanimoto coefficient. In order to evaluate this novel method, it was used to model three known and one unknown GPCR structures.

MATERIALS AND METHODS

Overview of Workflow. The workflow consists of two steps: (1) model construction and (2) assessment. The assessment step is divided into the following processes: (1) preparation of active ligands, (2) decoy generation, (3) docking simulation of active ligands and decoys, and (4) evaluation of models by discrimination scoring and consensus of PLIF of active ligands.

Step 1. Construction of Models. The target GPCR sequence was aligned with three GPCRs of known structure: human ADRB2 (PDB ID: 2RH1), bovine rhodopsin (OPSD, PDB ID: 1U19), and human adenosine receptor A2a (AA2AR, PDB ID: 3EML). Only three GPCR structures were available at the time of the study. The three structures were presuperimposed based on structural and sequence alignment using MOE 2009.10 (Chemical Computing Group). We selected several types of templates including single, multiple, and fragments from the above three known GPCR structures. Fragment-based modeling in this work is a template-based modeling method that differs from a general modeling approach with single or multiple template(s) in several important respects. A 3D model was constructed using coordinates from different templates for each transmembrane helix (TMH) region. In fragment-based modeling using three template GPCR structures, the target−structure alignment with all combinations of TMHs generates 2187 (= 3^7) candidate structures. However, some of the generated models were redundant because several TMH positions in the three templates were overlapped. To eliminate these redundant models, each set of template TMHs was divided into subsets based on the RMSDs of each pair of TMHs. The cutoff RMSD value was set at 2.5 Å (Figure 1). This cutoff value was defined by considering constrained computational resources in order to reduce the number of combinations of target−structure alignments used for model generation. After applying this threshold, 24 distinct alignment patterns remained (Table S2, Supporting Information). In addition to fragment-based modeling, single template modeling (using three patterns) and multiple templates modeling (using four patterns, three of which refer to two templates and one pattern which refers to all templates) were performed. The multiple template models constructed refer to different templates simultaneously, as with typical multiple template methods used in the MODELLER program.[24] This increased the number of distinct alignment patterns to 31. The second extracellular loop (ECL2) and the third intracellular loop (ICL3) regions were modeled by template-free modeling using the MODELLER program. The five residues leading out of TMH5 and the five residues leading into TMH6 in ICL3 were truncated because this loop is very long and was predicted to be disordered. We also introduced a disulfide bond constraint between cysteine residues in ECL2 and TMH3 in the modeling protocol if disulfide bond information was available in UniProt. Most class A GPCR

dx.doi.org/10.1021/ci500499j | J. Chem. Inf. Model. XXXX, XXX, XXX−XXX

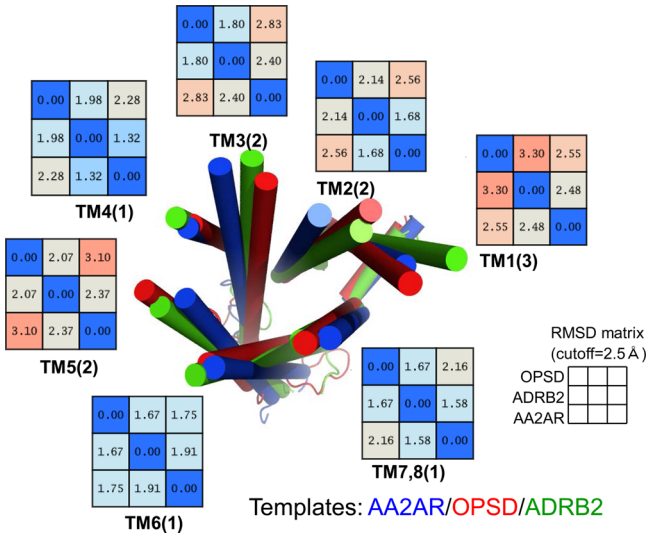

Figure 1. Overview of fragment-based modeling. This figure shows the TM helices of imposed templates viewed from the extracellular side. The RMSD tables of helices are shown alongside the structures. The combination pattern of templates is described in the Supporting Information.

structures have a conserved disulfide bond between cysteine residues in ECL2 and TMH3. Ten models for each target−template alignment were constructed using the MODELLER program. We generated 310 models for all target−template alignments.

For the OPRD, we tested a different template in addition to the above-mentioned templates. The human CXC chemokine receptor type 4 (CXCR4, PDB ID: 4EJ4) replaced AA2AR in the aforementioned triplets. The new templates used for the second validation were OPSD, ADRB2, and CXCR4. The construction procedure was exactly the same as that used for the above templates (OPSD, ADRB2, and AA2AR).

Step 2. Assessment of Models. *Preparation of Active Ligands.* Information regarding target GPCR active ligands was extracted from the DrugBank version 3.0 Web site (http://www.drugbank.ca/). DrugBank assigns ID numbers to known GPCR active ligands, as well as detailed annotation information including the 2D coordinates (SD files) of their structures. Clearly annotated active compounds were selected and then filtered using the Lipinski rules, that is, the number of acceptors ≤10, molecular weight ≤500, number of donors ≤5 and AlogP ≤ 5, because the decoy data were generated from a drug-like diverse subset of ZINC that was filtered using Lipinski's rule and was the only available diverse subset data at the time of the study. Suitable 3D coordinates, chirality, and states were generated using the Epik calculation with pH 7.0 on Ligprep. (Schrodinger, LLC, NY)

Decoy Generation for Docking Simulations. A decoy was generated from the ZINC database using the Directory of Useful Decoys (DUD)[25] method. First, a drug-like diverse subset clustered at 60% similarity was downloaded from the ZINC[26] Web site (http://zinc.docking.org/; version 10; property is the clean drug-like subset; this subset id is 13) Second, key fingerprints and the fingerprint-based similarity between the two data sets, that is, the ZINC data and the set of known active ligands obtained and prepared beforehand, were calculated using extended connectivity fingerprints (ECFP)[27] on Pipeline Pilot (Accerlys, Inc.). The data set with an ECFP similarity score less than 0.7 was selected to exclude topologically similar compounds. Third, descriptors based on the similarity determined using QickProp and QiqSim (Schrodinger, LLC, NY) were used to select the top 36 compounds with the highest similarity scores to known active ligands. Decoys were selected 36 times from the active ligands calculated from the ZINC data set using Ligprep. The number of final decoys was less than 36 times the number of active ligands because some ligands had the same decoys. The decoy was topologically dissimilar but had properties similar to the known actives. Finally, the possible states and chirality were calculated using Ligprep.

Docking of Active Ligands and Decoys. The constructed target GPCR models were refined for docking simulations using Protein Preparation Wizard Script into Maestro (Schrodinger, LLC, NY). Docking simulations were performed using Glide SP with default parameters (Schrodinger, LLC, NY). For Histamine HRH1, the van der Waals (vdW) radius was set to 0.7, and for the 5-hydroxytryptamine 2A serotonin receptor, the box size was set to 35 Å (length, width, height). Details are given in the Results and Discussion section. All models were superimposed on the ADRB2 X-ray structure (PDB ID: 2RH1) because the grid center of the models was defined in reference to the Carazolol center coordinate of this structure. Structures were superimposed using PyMol (Schrodinger, LLC).

Evaluation of Models. All models were evaluated using (1) ROC and AUC values for discrimination scoring, which are calculated docking scores of the active ligands and the decoys, and (2) the consensus of PLIF of the active ligands. PLIF is a fingerprint of the contact between a bound compound and protein residues. It is composed of an index and a value, where the index is the residue and the value is the number of contact atoms in the protein structure. The contact residue and the number of contacts are generated using the LIGPLOT[28] program. LIGPLOT counts the number of hydrogen bonds and nonbonded contacts per residue. In this work, the nonbonded contacts in the TMH regions were used to generate the PLIF because this approach included hydrogen bonds. The Tanimoto similarity score generated by the PLIF was calculated using the following equation

$$\mathrm{Tc} = \frac{\sum X_{i\mathrm{A}} X_{i\mathrm{B}}}{\sum (X_{i\mathrm{A}})^2 + \sum (X_{i\mathrm{B}})^2 - \sum X_{i\mathrm{A}} X_{i\mathrm{B}}}$$

where i is the number of the PLIF index, and X_i is the number of contact atoms in the index i residue. Tc is calculated for all combinations of compounds per model. If the model has a recognizable ligand binding mode, then the model compounds use the same common residue to bind to the protein structure. This process identifies a potential pharmacophore. In order to quantitatively rank the candidate binding positions, Tc50 was defined to be the lowest value of Tc among the top 50% of all PLIF pairs. A high Tc50 means that the selected model has a clearly defined pharmacophore that can be used for virtual screening.

PCA Analysis of Workflow Outcomes. The diversity of the models was evaluated using principal component analysis (PCA). To compare models with X-ray structures corresponding to template and actual target structures, the first and second principal components were calculated using the C alpha atom coordinates from only the TMH region of the crystallized protein structure. Principal component scores of the models

dx.doi.org/10.1021/ci500499j | J. Chem. Inf. Model. XXXX, XXX, XXX−XXX

were calculated based on the factor loadings of the X-ray structures.

RESULTS AND DISCUSSION

Validation of Our System Using Targets with Known and Unknown Structures. In order to evaluate the novel method presented herein, three targets with known three-dimensional structures, human DRD3, human HRH1, and human OPRD, were modeled, and the resulting structures were compared with the actual X-ray structures. As a more challenging target, we modeled the human HTR2A, whose structure is not known.

Known Structure Target 1: Result of DRD3 Obtained by Simple Workflow. The human DRD3 (PDB ID: 3PBL) structure was determined in 2010.[29] Structural models of DRD3 were constructed as per the workflow described above. The DRD3 amino acid sequence was obtained from UniProt. Three structures, ADRB2, OPSD, and AA2AR, were used as templates. The structural diversity of these DRD3 models was analyzed using principal component analysis (PCA). Principal components were calculated using the C alpha atoms in the TM regions of four X-ray structures and three templates, as well as a DRD3 X-ray structure that was not used as a template but was used to compare to the models. The principal component scores of the models were calculated using loading factors for these four structures. Figure 2a shows the result of PCA. The

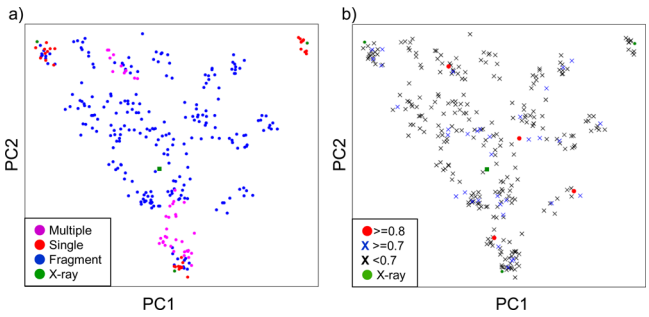

Figure 2. PCA of DRD3 models. These two plots are the same plot but colored according to different criteria. Panel (a) is colored according to the template. The green square plotted at the center indicates the DRD3 X-ray structure. The upper left green dot indicates AA2AR, upper right green dot indicates OPSD, and lower green dot indicates ADRB2. Panel (b) is colored according to the AUC value. The red points indicate models receiving AUC values over 0.8, blue x marks indicate models receiving AUC values over 0.7, and black crosses indicate models receiving AUC values under 0.7.

left plot (Figure 2a) is colored to indicate the different modeling methods employed. Three X-ray structures used as templates are plotted using green circular dots. The upper right green dot corresponds to OPSD, upper left dot corresponds to AA2AR, and bottom dot corresponds to ADRB2. The green square plotted in the center of the graph represents the DRD3 X-ray structure that was not utilized as a template. The fragment-based models (blue) were well spread out, not only around single (red) and multiple (magenta) templates but also distributed far from these areas. This method generated a large variety of structures near the actual X-ray structure. Fragment-based modeling is thus useful for increasing structural diversity. Figure 2b is colored according to the AUC values. Red outline dots represent the models with AUC values of 0.8 or more; blue crosses represent structures with AUC values more than 0.7 but less than 0.8, and black crosses represent structures with AUC values less than 0.7. Four models had high AUC values (more than 0.8, red solid dots in the right graph), but they were scattered over a large area. The model with the highest AUC value had a template pattern with multiples of ADRB2 and AA2AR that received the highest Tc50 scores. This best model (AUC = 0.85, Tc50 = 0.61) had higher AUC and Tc50 scores than the DRD3 X-ray structure (AUC = 0.75, Tc50 = 0.51). The docking pose of eticlopride is very similar to that revealed by the X-ray structure (Figure 3a,b). Furthermore, the contact

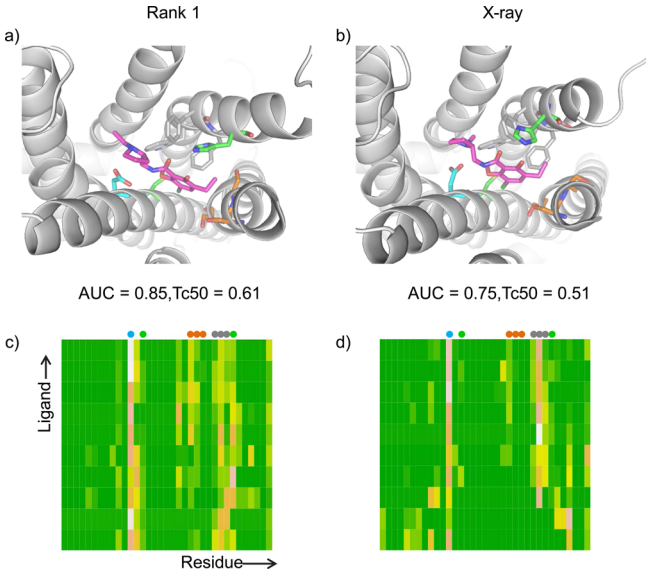

Figure 3. Evaluation results compared to the selected model and X-ray structure of DRD3. The left figures show the selected models, and the right figures correspond to the X-ray structure. The upper figures show the docking pose of the ligand and the contact residues. The contact residue is shown as sticks colored according to information from mutagenesis studies (see text). The bottom figures show the heat map from PLIF. The *x*-axis indicates the contact residue, and the *y*-axis indicates the ligands. The color represents the number of contacts. Deep green indicates no contact, and the colors shift gradually to yellow and then pale pink as the number of contacts increases. Colored dots on the heat map show the residue involved in ligand binding as verified by mutagenesis studies. The dot colors correspond to the residue colors in the upper figure. The best model (AUC = 0.85, Tc50 = 0.61) had a higher AUC and Tc50 than the DRD3 X-ray structure (AUC = 0.75, Tc50 = 0.51. If EL2 was removed, AUC = 0.51 and Tc50 = 0.50).

residues in the PLIF of the best model were consistent with results of mutagenesis studies. The highly conserved aspartic acid residue in TMH3 (D110 in DRD3, shown in stick representation with cyan carbon atoms in Figure 3a,b and as a cyan dot in Figure 3c,d) is critical for ligand binding.[29−31] Our PLIF results confirmed consensus contacts among active ligands and the protein. Cys114,[31] which is located only four residues away from D110 in TMH3 and His349[32] in TMH6, affects ligand binding (shown in stick representation with green carbon atoms and as a green dot in Figure 3). In addition, three serine residues (Ser192, S193, and S196 shown in stick representation with orange carbon atoms and as orange dots in Figure 3) are close together in TMH5 and play important accessory roles in agonist recognition and conformational change.[33] These mutation studies are consistent with our PLIF result. The consensus contacts of W342, F345, F346 (shown in

dx.doi.org/10.1021/ci500499j | J. Chem. Inf. Model. XXXX, XXX, XXX−XXX

stick representation with gray carbon atoms in Figure 3) in PLIF occur at the bottom of the ligand binding pocket. This is as predicted because W342 is part of a CWXP motif that is conserved in TMH6 of GPCRs. In the case of HRH1, two phenylalanine residues (which correspond to Y431 and F432 in HRH1) affect ligand binding.[34] (Figure 3c,d) These results demonstrated that our proposed workflow could generate and select a model that is even more structurally suitable for SBVS, in this validation test set, than the actual X-ray structure. The other study of a DRD3 homology model and SBVS reported that the model structure was more suitable for SBVS than the X-ray structure.[35] A new ligand was obtained from this homology model screening. This result illustrates the same tendency noted earlier, that the model structure performs better for SBVS than the X-ray structure.

Known Structure Target 2: HRH1 Required an Additional Parameter. The structure of human HRH1 (PDB ID: 3RZE) was reported in 2011.[36] Structural models were generated and analyzed as for DRD3. These models generated high AUC and high Tc50 scores, but similar models could not be obtained using a simple workflow. Three possible problems were considered as to why the models generated by a simple workflow did not generate high AUC and Tc50 scores. The first is that the partial alignments used in the simple workflow contained errors. The second is that atoms of the ligand crushed atoms of the receptor due to fluctuations of the side chains. The third is that the pocket shape of the model differed from the real pocket shape due to template selection errors. The first and second problems were related to the side chains. The third problem was related to the main chain. We addressed the first two problems as follows. We changed partial alignments by taking into account mutation studies that suggested W158 contributed to the binding pocket. The default alignment constructed by MOE contained a gap in TMH4 near W158. Therefore, the position of W158 was shifted into this gap region. Subsequently, the van der Waals (vdW) radii of the receptor atoms were reduced (receptor vdW scaling was set to 0.7, and ligand scaling was set to 0.8 as a default parameter) As a result of the first trial using a simple workflow, no residue has been confirmed by mutation studies to contact with active ligands during docking. The contact residues of the binding pose were placed at the extracellular side relative to the position of residues confirmed by mutation studies. We estimate that the binding pocket of HRH1 was deeper than the pockets of DRD3 and ADRB2. The deeper orthosteric binding pockets are condensed or narrowed owing to their funnel shape, which is a common structural feature of GPCRs. Therefore, slight movements of side chains caused the crush between ligand and receptor side chains. Developers of GLIDE have proposed a modification of the vdW scaling parameter on a case-by-case basis because the structure used for docking is applied to a rigid model, and in general, it has not been optimized to fit each ligand.[37,38] The vdW scaling parameter can be used to approximate slight movements of side chains at the binding pocket. This fluctuation, caused by the binding of different ligands, can be confirmed by the X-ray structures of ADRB2. There are seven representative structures of ADRB2 bound to different agonist and antagonist ligands, and these structures show that the side chains in the binding pocket do indeed fluctuate marginally.

Figure 4 shows the results of PCA, using the same color scheme as in Figure 2 for DRD3. Three X-ray structures used as templates are indicated by green circle dots. The upper right

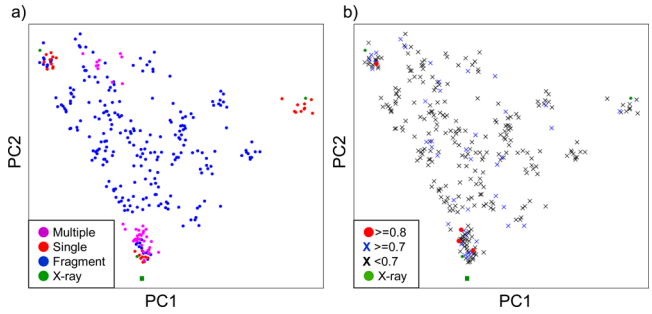

Figure 4. Result of PCA applied to HRH1. The principal component was defined by four X-ray structures (ADRB2, AA2AR, OPSD, and HRH1). Panel (a) is colored according to the template, and panel (b) is colored according to the AUC value. These colors are defined as in Figure 2.

green dot corresponds to OPSD, upper left dot corresponds to AA2AR, and bottom dot corresponds to ADRB2. The green square plotted below and slightly out of the area proscribed by these three templates represents the HRH1 X-ray structure, which was not utilized as a template. Four models scored high AUC values (over 0.8) and are scattered around the AA2AR X-ray structure and multiple templates area (Figure 4b). Only one of these four models was assigned a high Tc50 score (Tc50 $\geq$ 0.5). This selected model is the multiple template model of OPSD and ADRB2, and it scored the third highest AUC value. This model is very similar to the HRH1 X-ray structure; furthermore, among the four models with the highest AUC values, the RMSD of the X-ray structure, calculated from the C alpha atoms of the TM region, was only 1.25 Å. (RMSD are 1.33 Å in rank 1 models, 1.94 Å in rank 2 models, and 1.49 Å in rank 4 models) Figure 5 shows the heat map of PLIF and the docking pose of the active ligand. The ligand shown as a stick with a magenta carbon atom is the docking pose of doxepin in the HRH1 X-ray structure. The colored dots on the heat map

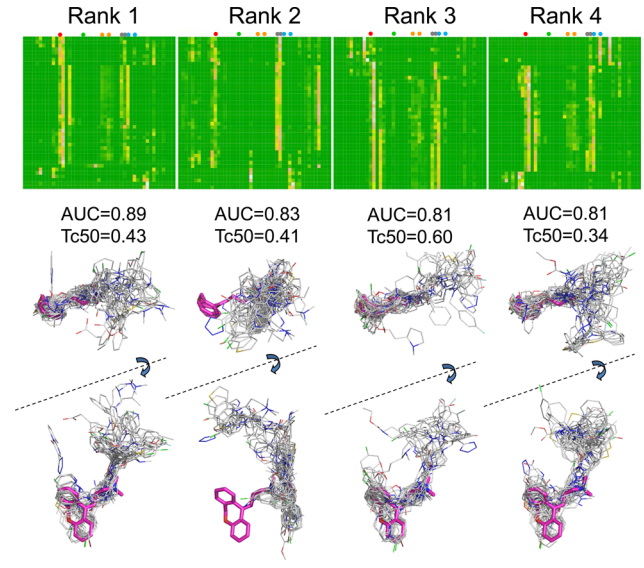

Figure 5. PLIF and docking pose of high AUC models. The upper figures are heat maps of PLIF, as in Figure 3. The colored dots represent residues known to contact the ligand. The lower figures show the docking pose of the active ligands and doxepin in the X-ray structures. Doxepin is colored magenta. Active ligands are colored gray.

dx.doi.org/10.1021/ci500499j | J. Chem. Inf. Model. XXXX, XXX, XXX−XXX

represent residues known by site-directed mutagenesis to contact the ligand. The red dot is the conserved aspartic acid (D107) in TMH3. The two orange dots are N198 and T194, which both partially effect ligand binding;[39] this was confirmed by partial contacts in the heat map. The guinea pig H1 receptor has a high sequence identity (72%) with human H1 receptor, and residues in the binding site are conserved with the human sequence. W158 (green dot in the heat maps in Figure 5) in TMH4 and two phenylalanine (F432 and F435, cyan dots in the heat map in Figure 5) in TMH6 are involved in ligand recognition, as confirmed by mutation studies in the guinea pig.[40] These residues, especially F432, contact many ligands in the selected model, whereas W158 and F435 contact a subset of those ligands. W428, which is part of the CWXP motif, and Y431 (gray dots in the heat maps in Figure5) are placed close together. These contacts are confirmed by the X-ray structure.

The model with the second-highest AUC value is plotted in the upper left region, far away from the other three models in the PCA plot (Figure 4b). The contact residues of this model were not consistent with mutagenesis studies. Known ligands were bound to different positions and not to the orthosteric binding site (Figure 5, rank 2). These results indicate that the AUC values did not correlate well with structural similarities. However, the use of the Tc50 and AUC values together resulted in elimination of false positives and selection of the best candidates for virtual screening.

Known Structure Target 3: OPRD Shows the Effect of a New Template Structure. The OPRD belongs to a peptide ligand subclass, class A, and its X-ray structure was solved in 2013.[41] Structural models were constructed according to the same workflow and analyzed using a simple workflow method. One model structure was assigned AUC values over 0.8, but no Tc50 values over 0.5 were obtained. We attribute this result to the different shapes of binding pockets; in other words, there was an error of template selection because the consensus contact could not be observed in the heat map of PLIF, whereas a few ligands could contact the receptor residues, as confirmed by mutation studies. We tried to replace AA2AR, one of three templates with human CXC chemokine receptor type 4 (CXCR4) whose structure was recently revealed,[42] and classified it into the same peptide ligand subclass as OPRD. Template replacement led to four models being assigned AUC values over 0.8. The second highest AUC model provided a Tc50 over 0.5.(AUC = 0.83, Tc50 = 0.69). The effect of the new template structure was also confirmed by the results of PCA (Figure 6). Four X-ray structures used as templates (ADRB2, AA2AR, OPSD, and CXCR4; CXCR4 was used instead of AA2AR in the second validation) and the human OPRD crystal structure were used to calculate principal components. These templates are shown as green dots in the PCA plots. The upper right green dot in Figure 6 corresponds to CXCR4, upper left green dot corresponds to AA2AR, bottom right green dot correspond to OPSD, and bottom left green dot corresponds to ADRB2. The green square plotted in the center of the graph represents the human OPRD X-ray structure that was not used as a template. In the first trial, ADRB2, OPSD, and AA2AR were used as templates (Figure 6a,c), but models could not be generated to cover the search area containing OPRD. The second trial did generate a model around the OPRD crystal structure because the search area can be changed due to the template replacement. The docking pose showed that active ligands that contain the same substructure as the ligands with known X-ray structures superposed well on the

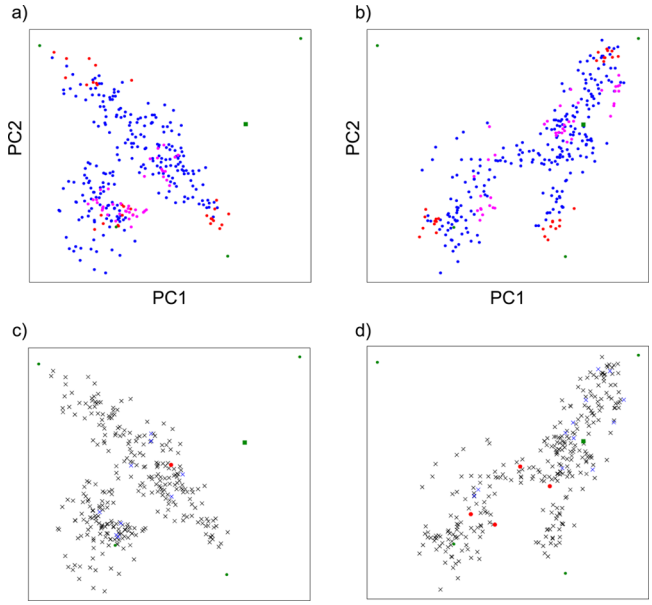

Figure 6. Result of PCA applied to OPRD. The green square plotted at the center indicates the human OPRD X-ray structure. The upper left green dot indicates AA2AR, upper right green dot indicates CXCR4, lower left green dot indicates ADRB2, and lower right green dot indicates OPSD. Panels (a) and (b) are colored according to the template, and panels (c) and (d) are colored according to the AUC value. These colors are defined as in Figures 2 and 4.

common substructure (Figure 7). Consensus contacts between the ligands and D128 are consistent with a site-directed

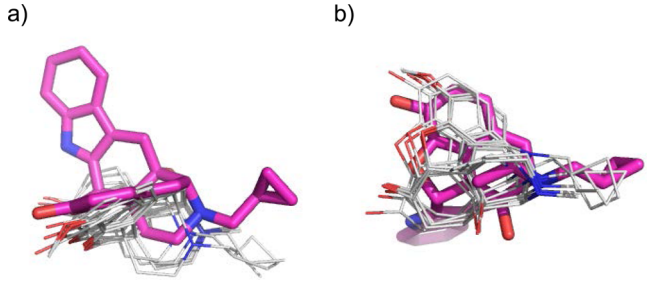

Figure 7. Docking pose of active ligands that have a substructure common to that of naltrindole in the best OPRD model structure selected by the second trial. The active ligands are colored gray. Naltrindole in the OPRD X-ray structure is colored magenta.

mutagenesis study.[43] There is no consensus contact between the ligand and three residues, W284, V296, and V297, known from a mutation study to be contact residues.[44] It seems reasonable that these residues, which are located on the extracellular side of the binding pocket, are involved in ligand selectivity and recognize a portion of the ligand called the "address". The "message-address" concept suggests that ligands are composed of two distinct modules carrying information about efficacy (message) and selectivity (address) in opioid pharmacology.[45,46] The lower portion of the binding pocket is well conserved in both sequence and structure among the opioid receptor subtypes and corresponds to the "message" part of recognition.[47] The aromatic residues located at the bottom of the binding pocket are consensus contacts observed by PLIF. The upper portion corresponds to the "address" part of recognition, and it differs between subtypes.[48] The active

dx.doi.org/10.1021/ci500499j | J. Chem. Inf. Model. XXXX, XXX, XXX−XXX

ligands utilized in this work have affinity for other opioid receptor subtypes, such as the μ and κ types.

Unknown Structure Target: Serotonin Receptor (5HT2A). A target with an unknown structure, human 5HT2A, was modeled using the same workflow and analyzed using the aforementioned methods. In the docking step, the grid box size was set larger (35 Å^2) than the default value because the known active ligands of 5HT2A are larger than in the above three cases. Other procedures were the same as in the earlier simple workflow. Figure 8 shows the results for PCA,

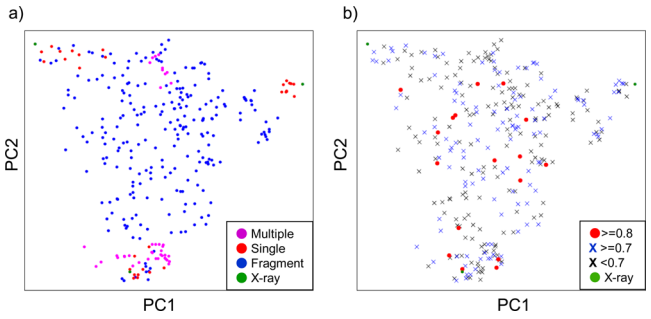

Figure 8. Result of PCA applied to HTR2A. Panel (a) is colored according to the template, and panel (b) is colored according to the AUC value. These colors are defined as in Figures 2 and 4.

colored using the same scheme as in Figure 2 for DRD3. The three X-ray structures used as templates are indicated by green circle dots. The upper right green dot corresponds to OPSD, upper left green dot corresponds to AA2AR, and bottom green dot corresponds to ADRB2. The docking evaluation produced 17 models with AUC values greater than 0.8. These are distributed widely in the PCA plot (Figure 8b). The highest AUC scoring model (AUC = 0.88) had a Tc50 score over 0.5 (Tc50 = 0.54). The modeling method producing this target candidate was fragment-based, and the combination pattern ID of its templates was 21 (Table S2, Supporting Information). An aspartic acid residue in TMH3 critical for contact[49] was confirmed as a contact residue by PLIF. The contact residues detected by PLIF were consistent with mutagenesis experiments.

General Discussion. In general, constructed models are assessed using AUC for their ability to discriminate between active ligands and decoys. The model with the highest AUC is considered to be the best and thus is usually selected for virtual screening. Does the highest AUC value indeed indicate the best model of a candidate pharmacophore for virtual screening? It is important to select the most suitable model for virtual screening from a number of candidates having high AUC values; hence, the docking poses of active compounds were evaluated using PLIF. If these active ligands bind to orthosteric binding sites, then the residues participating in this binding interaction should be consistent with the results of site-directed mutagenesis studies. In fact, the Tc50 values for seven X-ray structures of ADRB2 that were cocrystallized with an inverse agonist, an antagonist, or an agonist were very high (Tc50 = 0.74). As a result of evaluation by both AUC and Tc50, the most suitable candidate for virtual screening could be selected. Tc50 could be applied to a set of active ligands that contain dissimilar ligands because this indicator does not measure the similarity of ligands but rather the consensus of the contact residue (Figure S1, Supporting Information).

At the beginning of our study, only three representative structures (ADRB2, AA2AR, and OPSD) were available as templates. However, many GPCR structures have been released recently, allowing us to test CXCR4 as a newer structure and determine the effect of this new template for OPRD. We found that it worked well. This newer structure was useful for broadening the model search area, but the problem remains of how to select templates from the 24 representative X-ray structures. In the case of OPRD, when CXCR4 instead of AA2AR was used as a template, it worked well because (1) it belongs to the same peptide subfamily as OPRD and (2) it has a larger binding pocket relative to the original three templates. The larger binding pocket is a common feature of this peptide subfamily. It is likely that one of the three templates chosen is from the same subfamily as the target and that the other two templates chosen belong to another subfamily because the search area of the model structure had to be expanded. Furthermore, by coordinating with the GPCR-SSFE template selection workflow, this template selection scheme may be further improved and automated.

CONCLUSIONS

This study reports an extended template-based modeling method and an evaluation method for SBVS, both of which are specialized for GPCRs. The modeling steps are composed of three methods that utilize single, multiple, and fragment-based templates. The evaluation steps are based on consensus of the ligand docking pose using protein ligand interaction fingerprints that were produced by ligand−protein docking simulations. In order to evaluate this system, four targets, DRD3, HRH1, OPRD, and HTR2A, were analyzed. The first three targets had known X-ray structures, while the fourth one had an unknown structure.

Worth et al. analyzed the relationship between GPCR structures and sequences for template selection to construct structural models.[18] They concluded that sequence similarities among the TM regions were not sufficient to select the optimal templates. Interestingly, the template patterns of our selected models did not always match their sequence similarity scores. Multiple and fragment-based modeling fits well into this workflow. This workflow contains ROC (AUC) and PLIF (Tc50) to evaluate optimum candidate structures in the evaluation step. Tc50 values also provided valuable indicators of consensus binding modes. The most suitable model was then selected by combining these methods with analysis of AUC values, thus improving the discrimination between candidate structures. These could further be utilized as starting structures for molecular dynamics (MD) simulations, which require reliable structures close to the actual three-dimensional structure to remove artifacts and decrease the computer time required for MD-based optimizations.

ASSOCIATED CONTENT

Supporting Information

Tables S1, S2, and S3 and Figure S1. This material is available free of charge via the Internet at http://pubs.acs.org.

AUTHOR INFORMATION

Corresponding Author

*E-mail: t-hirokawa@aist.go.jp.

Notes

The authors declare no competing financial interest.

dx.doi.org/10.1021/ci500499j | J. Chem. Inf. Model. XXXX, XXX, XXX−XXX

■ ACKNOWLEDGMENTS

We express the greatest appreciation to Professor Akinori Kidera, Associate Professor Mitsunori Ikeguchi, and Research Associate Sotaro Fuchigami for thoughtful discussions. This work was partially supported by Platform for Drug Discovery, Informatics, and Structural Life Science from the Ministry of Education, Culture, Sports, Science and Technology, Japan.

■ REFERENCES

(1) Lagerstrom, M. C.; Schioth, H. B. Structural diversity of G protein-coupled receptors and significance for drug discovery. *Nat. Rev. Drug Discovery* **2008**, *7*, 339−57.
(2) Venkatakrishnan, A. J.; Deupi, X.; Lebon, G.; Tate, C. G.; Schertler, G. F.; Babu, M. M. Molecular signatures of G-protein-coupled receptors. *Nature* **2013**, *494*, 185−94.
(3) Wang, C.; Jiang, Y.; Ma, J.; Wu, H.; Wacker, D.; Katritch, V.; Han, G. W.; Liu, W.; Huang, X. P.; Vardy, E.; McCorvy, J. D.; Gao, X.; Zhou, X. E.; Melcher, K.; Zhang, C.; Bai, F.; Yang, H.; Yang, L.; Jiang, H.; Roth, B. L.; Cherezov, V.; Stevens, R. C.; Xu, H. E. Structural basis for molecular recognition at serotonin receptors. *Science* **2013**, *340*, 610−4.
(4) Wacker, D.; Wang, C.; Katritch, V.; Han, G. W.; Huang, X. P.; Vardy, E.; McCorvy, J. D.; Jiang, Y.; Chu, M.; Siu, F. Y.; Liu, W.; Xu, H. E.; Cherezov, V.; Roth, B. L.; Stevens, R. C. Structural features for functional selectivity at serotonin receptors. *Science* **2013**, *340*, 615−9.
(5) Tan, Q.; Zhu, Y.; Li, J.; Chen, Z.; Han, G. W.; Kufareva, I.; Li, T.; Ma, L.; Fenalti, G.; Zhang, W.; Xie, X.; Yang, H.; Jiang, H.; Cherezov, V.; Liu, H.; Stevens, R. C.; Zhao, Q.; Wu, B. Structure of the CCR5 chemokine receptor-HIV entry inhibitor maraviroc complex. *Science* **2013**, *341*, 1387−90.
(6) Tse, M. T. G protein-coupled receptors: Two landmark class B GPCR structures unveiled. *Nat. Rev. Drug Discovery* **2013**, *12*, 579.
(7) Wang, C.; Wu, H.; Katritch, V.; Han, G. W.; Huang, X. P.; Liu, W.; Siu, F. Y.; Roth, B. L.; Cherezov, V.; Stevens, R. C. Structure of the human smoothened receptor bound to an antitumour agent. *Nature* **2013**, *497*, 338−43.
(8) Wu, H.; Wang, C.; Gregory, K. J.; Han, G. W.; Cho, H. P.; Xia, Y.; Niswender, C. M.; Katritch, V.; Meiler, J.; Cherezov, V.; Conn, P. J.; Stevens, R. C. Structure of a class C GPCR metabotropic glutamate receptor 1 bound to an allosteric modulator. *Science* **2014**, *344*, 58−64.
(9) Zhang, J.; Zhang, K.; Gao, Z. G.; Paoletta, S.; Zhang, D.; Han, G. W.; Li, T.; Ma, L.; Zhang, W.; Muller, C. E.; Yang, H.; Jiang, H.; Cherezov, V.; Katritch, V.; Jacobson, K. A.; Stevens, R. C.; Wu, B.; Zhao, Q. Agonist-bound structure of the human P2Y12 receptor. *Nature* **2014**, *509*, 119−22.
(10) Pierce, K. L.; Premont, R. T.; Lefkowitz, R. J. Seven-transmembrane receptors. *Nat. Rev. Mol. Cell Biol.* **2002**, *3*, 639−50.
(11) Shacham, S.; Marantz, Y.; Bar-Haim, S.; Kalid, O.; Warshaviak, D.; Avisar, N.; Inbal, B.; Heifetz, A.; Fichman, M.; Topf, M.; Naor, Z.; Noiman, S.; Becker, O. M. PREDICT modeling and in-silico screening for G-protein coupled receptors. *Proteins* **2004**, *57*, 51−86.
(12) Vaidehi, N.; Floriano, W. B.; Trabanino, R.; Hall, S. E.; Freddolino, P.; Choi, E. J.; Zamanakos, G.; Goddard, W. A., 3rd Prediction of structure and function of G protein-coupled receptors. *Proc. Natl. Acad. Sci. U. S. A.* **2002**, *99*, 12622−7.
(13) Abrol, R.; Bray, J. K.; Goddard, W. A., 3rd. Bihelix: Towards de novo structure prediction of an ensemble of G-protein coupled receptor conformations. *Proteins* **2011**, DOI: 10.1002/prot.23216.
(14) Ananthan, S.; Zhang, W.; Hobrath, J. V. Recent advances in structure-based virtual screening of G-protein coupled receptors. *AAPS J.* **2009**, *11*, 178−85.
(15) Larsson, P.; Wallner, B.; Lindahl, E.; Elofsson, A. Using multiple templates to improve quality of homology models in automated homology modeling. *Protein Sci.* **2008**, *17*, 990−1002.
(16) Mobarec, J. C.; Sanchez, R.; Filizola, M. Modern homology modeling of G-protein coupled receptors: which structural template to use? *J. Med. Chem.* **2009**, *52*, 5207−16.
(17) Worth, C. L.; Kreuchwig, A.; Kleinau, G.; Krause, G. GPCR-SSFE: A comprehensive database of G-protein-coupled receptor template predictions and homology models. *BMC Bioinf.* **2011**, *12*, 185.
(18) Worth, C. L.; Kleinau, G.; Krause, G. Comparative sequence and structural analyses of G-protein-coupled receptor crystal structures and implications for molecular models. *PLoS One* **2009**, *4*, e7011.
(19) Evers, A.; Hessler, G.; Matter, H.; Klabunde, T. Virtual screening of biogenic amine-binding G-protein coupled receptors: comparative evaluation of protein- and ligand-based virtual screening protocols. *J. Med. Chem.* **2005**, *48*, 5448−65.
(20) de Graaf, C.; Rognan, D. Selective structure-based virtual screening for full and partial agonists of the beta2 adrenergic receptor. *J. Med. Chem.* **2008**, *51*, 4978−85.
(21) Wacker, D.; Fenalti, G.; Brown, M. A.; Katritch, V.; Abagyan, R.; Cherezov, V.; Stevens, R. C. Conserved binding mode of human beta2 adrenergic receptor inverse agonists and antagonist revealed by X-ray crystallography. *J. Am. Chem. Soc.* **2010**, *132*, 11443−5.
(22) Kobilka, B. K.; Deupi, X. Conformational complexity of G-protein-coupled receptors. *Trends Pharmacol. Sci.* **2007**, *28*, 397−406.
(23) Granier, S.; Kobilka, B. A new era of GPCR structural and chemical biology. *Nat. Chem. Biol.* **2012**, *8*, 670−3.
(24) Sali, A.; Blundell, T. L. Comparative protein modelling by satisfaction of spatial restraints. *J. Mol. Biol.* **1993**, *234*, 779−815.
(25) Huang, N.; Shoichet, B. K.; Irwin, J. J. Benchmarking sets for molecular docking. *J. Med. Chem.* **2006**, *49*, 6789−801.
(26) Irwin, J. J.; Shoichet, B. K. ZINC—A free database of commercially available compounds for virtual screening. *J. Chem. Inf. Model* **2005**, *45*, 177−82.
(27) Rogers, D.; Hahn, M. Extended-connectivity fingerprints. *J. Chem. Inf. Model* **2010**, *50*, 742−54.
(28) Wallace, A. C.; Laskowski, R. A.; Thornton, J. M. LIGPLOT: A program to generate schematic diagrams of protein-ligand interactions. *Protein Eng.* **1995**, *8*, 127−34.
(29) Chien, E. Y.; Liu, W.; Zhao, Q.; Katritch, V.; Han, G. W.; Hanson, M. A.; Shi, L.; Newman, A. H.; Javitch, J. A.; Cherezov, V.; Stevens, R. C. Structure of the human dopamine D3 receptor in complex with a D2/D3 selective antagonist. *Science* **2010**, *330*, 1091−5.
(30) Shi, L.; Javitch, J. A. The binding site of aminergic G protein-coupled receptors: the transmembrane segments and second extracellular loop. *Annu. Rev. Pharmacol. Toxicol.* **2002**, *42*, 437−67.
(31) Alberts, G. L.; Pregenzer, J. F.; Im, W. B. Contributions of cysteine 114 of the human D3 dopamine receptor to ligand binding and sensitivity to external oxidizing agents. *Br. J. Pharmacol.* **1998**, *125*, 705−10.
(32) Lundstrom, K.; Turpin, M. P.; Large, C.; Robertson, G.; Thomas, P.; Lewell, X. Q. Mapping of dopamine D3 receptor binding site by pharmacological characterization of mutants expressed in CHO cells with the Semliki Forest virus system. *J. Recept. Signal Transduction Res.* **1998**, *18*, 133−50.
(33) Sartania, N.; Strange, P. G. Role of conserved serine residues in the interaction of agonists with D3 dopamine receptors. *J. Neurochem.* **1999**, *72*, 2621−4.
(34) Jongejan, A.; Leurs, R. Delineation of receptor−ligand interactions at the human histamine H1 receptor by a combined approach of site-directed mutagenesis and computational techniques - or - how to bind the H1 receptor. *Arch. Pharm. (Weinheim, Ger.)* **2005**, *338*, 248−59.
(35) Carlsson, J.; Coleman, R. G.; Setola, V.; Irwin, J. J.; Fan, H.; Schlessinger, A.; Sali, A.; Roth, B. L.; Shoichet, B. K. Ligand discovery from a dopamine D3 receptor homology model and crystal structure. *Nat. Chem. Biol.* **2011**, *7*, 769−78.
(36) Shimamura, T.; Shiroishi, M.; Weyand, S.; Tsujimoto, H.; Winter, G.; Katritch, V.; Abagyan, R.; Cherezov, V.; Liu, W.; Han, G. W.; Kobayashi, T.; Stevens, R. C.; Iwata, S. Structure of the human histamine H1 receptor complex with doxepin. *Nature* **2011**, *475*, 65−70.

(37) Friesner, R. A.; Banks, J. L.; Murphy, R. B.; Halgren, T. A.; Klicic, J. J.; Mainz, D. T.; Repasky, M. P.; Knoll, E. H.; Shelley, M.; Perry, J. K.; Shaw, D. E.; Francis, P.; Shenkin, P. S. Glide: A new approach for rapid, accurate docking and scoring. 1. Method and assessment of docking accuracy. *J. Med. Chem.* **2004**, *47*, 1739−49.
(38) Halgren, T. A.; Murphy, R. B.; Friesner, R. A.; Beard, H. S.; Frye, L. L.; Pollard, W. T.; Banks, J. L. Glide: a new approach for rapid, accurate docking and scoring. 2. Enrichment factors in database screening. *J. Med. Chem.* **2004**, *47*, 1750−9.
(39) Ohta, K.; Hayashi, H.; Mizuguchi, H.; Kagamiyama, H.; Fujimoto, K.; Fukui, H. Site-directed mutagenesis of the histamine H1 receptor: roles of aspartic acid107, asparagine198 and threonine194. *Biochem. Biophys. Res. Commun.* **1994**, *203*, 1096−101.
(40) Wieland, K.; Laak, A. M.; Smit, M. J.; Kuhne, R.; Timmerman, H.; Leurs, R. Mutational analysis of the antagonist-binding site of the histamine H(1) receptor. *J. Biol. Chem.* **1999**, *274*, 29994−30000.
(41) Fenalti, G.; Giguere, P. M.; Katritch, V.; Huang, X. P.; Thompson, A. A.; Cherezov, V.; Roth, B. L.; Stevens, R. C. Molecular control of delta-opioid receptor signalling. *Nature* **2014**, *506*, 191−6.
(42) Wu, B.; Chien, E. Y.; Mol, C. D.; Fenalti, G.; Liu, W.; Katritch, V.; Abagyan, R.; Brooun, A.; Wells, P.; Bi, F. C.; Hamel, D. J.; Kuhn, P.; Handel, T. M.; Cherezov, V.; Stevens, R. C. Structures of the CXCR4 chemokine GPCR with small-molecule and cyclic peptide antagonists. *Science* **2010**, *330*, 1066−71.
(43) Befort, K.; Tabbara, L.; Bausch, S.; Chavkin, C.; Evans, C.; Kieffer, B. The conserved aspartate residue in the third putative transmembrane domain of the delta-opioid receptor is not the anionic counterpart for cationic opiate binding but is a constituent of the receptor binding site. *Mol. Pharmacol.* **1996**, *49*, 216−23.
(44) Valiquette, M.; Vu, H. K.; Yue, S. Y.; Wahlestedt, C.; Walker, P. Involvement of Trp-284, Val-296, and Val-297 of the human delta-opioid receptor in binding of delta-selective ligands. *J. Biol. Chem.* **1996**, *271*, 18789−96.
(45) Chavkin, C.; Goldstein, A. Specific receptor for the opioid peptide dynorphin: Structure−activity relationships. *Proc. Natl. Acad. Sci. U.S.A.* **1981**, *78*, 6543−7.
(46) Lipkowski, A. W.; Tam, S. W.; Portoghese, P. S. Peptides as receptor selectivity modulators of opiate pharmacophores. *J. Med. Chem.* **1986**, *29*, 1222−5.
(47) Befort, K.; Tabbara, L.; Kling, D.; Maigret, B.; Kieffer, B. L. Role of aromatic transmembrane residues of the delta-opioid receptor in ligand recognition. *J. Biol. Chem.* **1996**, *271*, 10161−8.
(48) Granier, S.; Manglik, A.; Kruse, A. C.; Kobilka, T. S.; Thian, F. S.; Weis, W. I.; Kobilka, B. K. Structure of the delta-opioid receptor bound to naltrindole. *Nature* **2012**, *485*, 400−4.
(49) Almaula, N.; Ebersole, B. J.; Zhang, D.; Weinstein, H.; Sealfon, S. C. Mapping the binding site pocket of the serotonin 5-hydroxytryptamine2A receptor. Ser3.36(159) provides a second interaction site for the protonated amine of serotonin but not of lysergic acid diethylamide or bufotenin. *J. Biol. Chem.* **1996**, *271*, 14672−5.